

Longshore Current on a Barred Beach: Field Measurements and Calculation

JANE MCKEE SMITH

U.S. Army Engineer Waterways Experiment Station, Coastal Engineering Research Center, Vicksburg, Mississippi

MAGNUS LARSON

Department of Water Resources Engineering, University of Lund, Lund, Sweden

NICHOLAS C. KRAUS¹

Conrad Blucher Institute for Surveying and Science, Texas A&M University–Corpus Christi

Measurements of the longshore current on a barred beach made during the 1990 Duck Experiment on Low-Frequency and Incident-Band Longshore and Across-Shore Hydrodynamics (DELILAH) field data collection project conducted at Duck, North Carolina, revealed an unexpected and persistent broad peak in the current velocity in the trough between the nearshore bar and the shore. This paper introduces longshore current and associated wave measurements from DELILAH together with a numerical model capable of describing the field observations. An existing numerical model of the mean current is modified to include a general transport equation for the mean turbulent kinetic energy created by wave breaking, and Reynolds stress components needed to calculate the longshore current and mean water level are reexpressed to include the turbulent momentum transport. In comparison to predictions from the original model, the modified model produces much improved agreement with the measured current velocity on the barred profiles in the field measurements and with the velocity profile and mean water level generated on a uniformly sloping laboratory beach by monochromatic waves. Three forms of a bottom friction coefficient are examined, and the open-channel-flow Manning friction coefficient is selected because of best agreement and consistency. Values of the Manning friction coefficient required to calibrate the model agree with values normally assigned to the related bottom roughness in open-channel flow.

INTRODUCTION

Recent reviews of the theory and measurement of the time-mean longshore current [Komar and Oltman-Shay, 1990; Kraus and Larson, 1991 (hereinafter referred to as KL)] have indicated that the accepted radiation stress theory of the longshore current satisfactorily describes the cross-shore distribution of the current both in the laboratory and in the field for uniformly sloping beaches. We note, however, that there is a tendency for the predicted peak in the current distribution to be located seaward of the measured peak in many studies cited in these reviews. The implication from the reviews is that the theory carries over to barred profiles; indeed, several analytic and numerical models of the longshore current on a barred profile have been developed [Ebersole and Dalrymple, 1980; Symonds and Huntley, 1980; Baum and Basco, 1986; Larson and Kraus, 1991 (hereinafter referred to as LK)], of which the model by LK, discussed below, is among the most sophisticated and complete of such one-dimensional models (where “one-dimensional” refers to a depth-averaged current with longshore uniformity in depth, waves, and current). These previous models for barred beach profiles, which couple four main governing equations (defining a four-equation model)

for the wave height, wave angle, mean water surface elevation, and longshore current across the nearshore, universally predict a local peak in the current located at or somewhat shoreward of a bar crest, where the gradient in wave height is maximum. They also predict a broad near-constant minimum (usually zero) in the current in the trough where waves reform after breaking on the bar and a second peak in the current at the shoreline where the reformed waves break. Until recently, high-quality data to confirm the predictions of four-equation models for barred beaches were lacking. Dense measurements of the longshore current on a barred profile obtained in the 1990 DELILAH field data collection project (described below) frequently show a large and broad peak in the longshore current velocity well within the trough that would be considered extraordinarily anomalous in a four-equation modeling system. Examination of the extensive DELILAH data set indicates that the presence of a broad peak in the current on the barred profile at Duck is typical. Allender *et al.* [1978] reported similar current patterns on the barred profile near Zion, Illinois, in Lake Michigan.

Quantitative prediction of the longshore current on barred profiles is required for understanding longshore sand transport and beach evolution. Cross-shore gradients in the longshore current distribution generated by short-period incident waves drive longer-period current motions termed shear or instability waves [Bowen and Holman, 1989; Oltman-Shay *et al.*, 1989], and Howd *et al.* [1991] have posited that edge wave modification by a strong longshore current may contribute to bar migration, indicating that accurate

¹Formerly at U.S. Army Engineer Waterways Experiment Station, Coastal Engineering Research Center, Vicksburg, Mississippi.

Copyright 1993 by the American Geophysical Union.

Paper number 93JC02116.
0148-0227/93/93JC-02116\$05.00

calculation of the longshore current is required to predict the large-scale current pattern and beach morphology change.

In addition to disparities between the predicted and measured longshore currents on barred beaches, precise measurements of setdown under monochromatic breaking waves on a uniformly sloping beach in the laboratory have indicated that the point of maximum setdown lies shoreward of the breakpoint [e.g., *Bowen et al.*, 1968; *Van Dorn*, 1976], and the region of maximum setdown can appear broad and flat rather than as a distinct, sharp minimum in the water level. *Visser* [1982, 1991] performed careful laboratory experiments to measure wave height, mean water surface elevation, and the longshore current produced by monochromatic waves on a uniformly sloping beach. *Visser* [1984] obtained improved agreement in reproducing the locations of the measured maximum setdown and the peak in the longshore current distribution with a four-equation model of setdown and current if he constrained the onset of wave dissipation in the model to commence at the plunge point of the breaking waves rather than at the breakpoint. The rationale was that waves in the "transition region" [*Svendsen et al.*, 1978; *Svendsen*, 1984] between the breakpoint and plunge point, where the wave overturns as an organized body or roller [*Sawaragi and Iwata*, 1974], undergo a steep decrease in height but not a correspondingly great increase in wave energy dissipation. *Roelvink and Stive* [1989] thereafter distinguished between the production of turbulence from organized wave energy through the energy balance equation and the dissipation of mean turbulent kinetic energy (TKE) calculated in a one-equation TKE transport model in which the production term for the TKE is taken from the wave energy balance equation. *Nairn et al.* [1990] and *Deigaard et al.* [1991] also applied a one-equation TKE transport model with the governing hydrodynamic equations to obtain an improved description of the mean water surface elevation and undertow.

In this paper, we present high-quality, comprehensive field measurements from the DELILAH project of the wave height and mean longshore current over a barred beach profile. The longshore current model of LK is modified to include a general transport equation for the TKE generated under breaking waves, and a consistent method for calculating the mean water surface elevation and longshore current by including turbulent transport in the momentum equations is presented. Predictions of wave height and current obtained with this five-equation model (equations for the wave height, wave angle, turbulent kinetic energy, longshore current, and mean water level) are compared with the field data, for which the wave input is provided by an individual wave height model run in random mode through Monte Carlo selection [LK]. Additional verification of the model is made with the *Visser* [1982] laboratory measurements of the longshore current distribution and mean water surface elevation generated by monochromatic waves arriving obliquely to a uniformly sloping beach. The field data are introduced first to motivate the need for an improved mathematical model of the longshore current.

FIELD OBSERVATIONS: DELILAH FIELD DATA COLLECTION PROJECT

In October 1990 a multiinstitutional cooperative field data collection project named DELILAH (Duck Experiment on

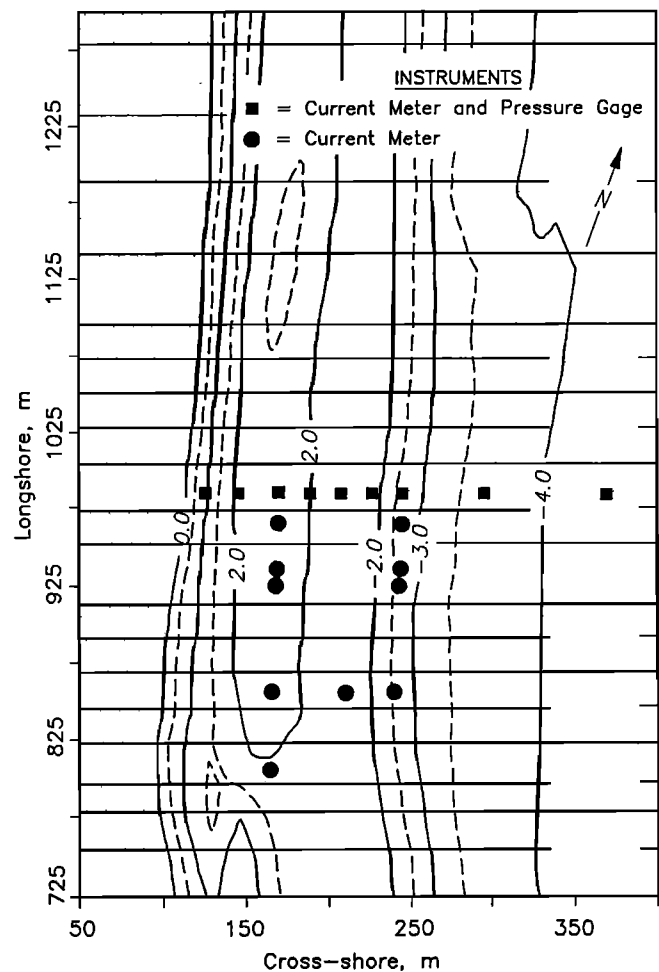


Fig. 1. Plan view of instrument locations during DELILAH.

Low-frequency and Incident-band Longshore and Across-shore Hydrodynamics) was conducted on the barred near-shore bathymetry at the U.S. Army Engineer Waterways Experiment Station, Coastal Engineering Research Center, Field Research Facility (FRF) located in Duck, North Carolina, which faces the Atlantic Ocean on a long, sandy, barrier island beach. The objectives of the DELILAH project were to measure the wave- and wind-forced three-dimensional nearshore dynamics (with emphasis on infragravity waves, shear waves, mean circulation, setup, runup, and wave transformation) and to monitor the bathymetric response to the operating hydrodynamic processes. A dense array of current meters and pressure gages was deployed in the nearshore during the period October 1–19, 1990. The experiment provided detailed synoptic measurement of nearshore mean currents as well as of the conditions generating the currents: nearshore waves, wind, tide, and bathymetry.

Nineteen electromagnetic current meters and nine pressure gages were deployed in water depths of 4 m to less than 1 m from 250 m offshore to the shoreline. The instruments were arranged in a primary cross-shore array of colocated pressure gages and current meters at nine locations and two secondary longshore arrays of current meters (50 and 125 m offshore) as shown in Figure 1. The current meters and pressure gages were mounted on pipes jetted into the sand, and the current meter sensors were mounted on standoffs

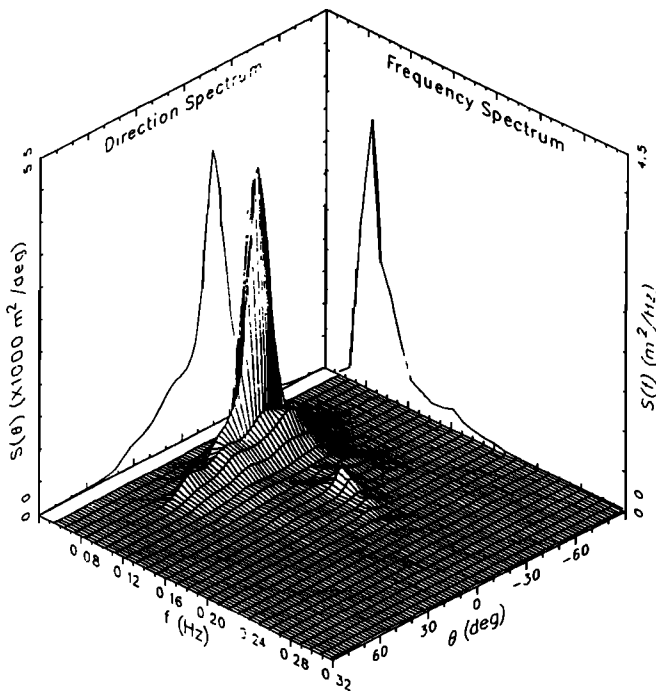


Fig. 2. Wave spectrum measured in 8-m water depth on October 14, 1990, at 1900 EST.

from these pipes to reduce flow interference. The current meters were calibrated before and after the project, with changes in gain of less than 5% and changes in offset of 0 to 6 cm s^{-1} for the cross-shore array. Nearshore wave and current data were collected continuously at a sampling rate of 8 Hz throughout the experiment. This paper focuses on

the data from the primary cross-shore array which contains both wave and current measurements.

Offshore waves were measured with an array of 16 pressure gages at the 8-m depth contour. High-resolution spectra were calculated from the array data every 3 hours for the experiment duration using the iterative maximum likelihood method [Pawka, 1983]. These directional data provide offshore boundary conditions for wave forcing of the numerical model. Over-water winds and tidal elevation were measured at the FRF pier. The bathymetry in the area of the nearshore current meter/pressure gage array (340- by 600-m area) was surveyed daily during DELILAH by a self-contained vehicle (the coastal research amphibious buggy, or CRAB) driven along survey transects. The position and elevation of the CRAB were determined with a Geodimeter autotracking electronic total station that provides high-spatial resolution and accuracy. The median sediment grain size in the FRF nearshore varies from 0.7 mm on the steep foreshore to 0.2 mm on the bar and 0.12 mm in the offshore [Howd and Birkemeier, 1987].

For investigating the longshore current, we examine measurements taken on October 14. On this day the wave spectra measured at the 8-m depth were narrow banded in frequency with symmetric directional distributions about a mean oblique wave direction. Figure 2 shows an example of the two-dimensional (frequency-direction) wave spectrum measured on October 14. In this figure the vertical axis is the energy density $S(f, \theta)$, and the horizontal axes are wave frequency f and direction θ . The unimodal swell wave trains are favorable for modeling wave transformation with linear wave propagation. On October 14 the significant wave height at the 8-m gage depth was 1.1 to 1.5 m with a peak period of 10 to 12 s and a mean direction of 10° to 30° south of shore normal. The bathymetry was nearly uniform alongshore, as shown in Figure 3.

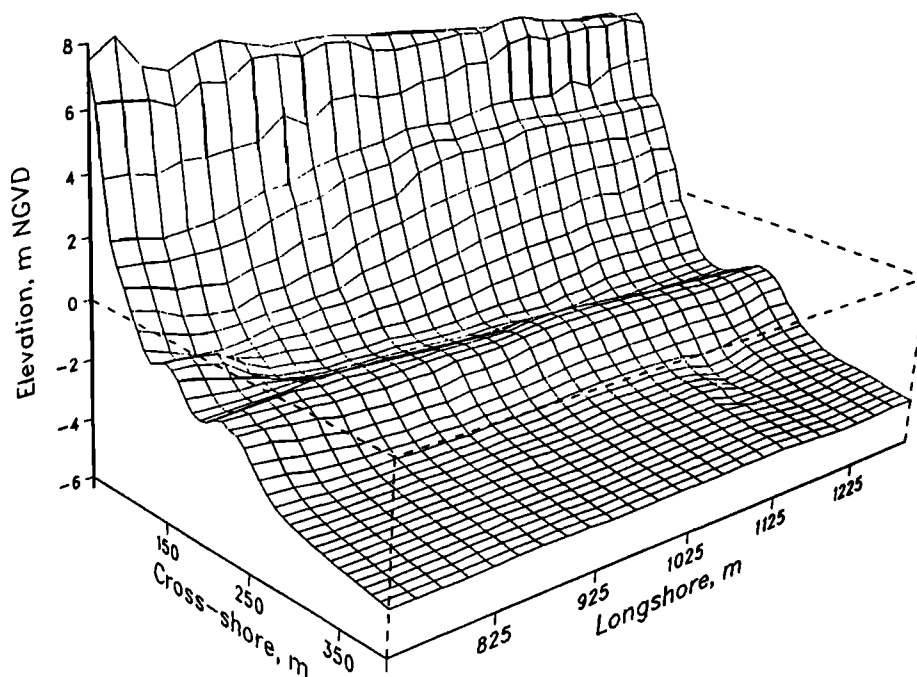


Fig. 3. Nearshore bathymetry at the Field Research Facility on October 14, 1990, relative to the National Geodetic Vertical Datum (NGVD).

NUMERICAL MODEL

The four-equation wave transformation and longshore current model, including the numerical solution schemes and verification with field and laboratory data for uniformly and nearly uniformly sloping beaches, has been described by KL and LK. In this section we review the model and introduce the TKE transport equation. Assumptions typical in longshore current modeling are made, of which the principal ones are (1) longshore uniformity in waves, wind, and bottom topography, (2) stationarity of wave conditions, (3) applicability of linear-wave theory, (4) neglect of bottom friction in the cross-shore plane, and (5) applicability of standard closure relations (to be discussed).

Wave Model

The wave model employs a modified version of the *Dally et al.* [1985] (hereinafter referred to as D3) model for wave decay and reformation after breaking. The D3 model was generalized by LK to describe oblique wave incidence over irregular profiles with parallel contours, including a barred profile, as

$$\frac{dF_x}{dx} = \frac{\kappa}{d} (F - F_s) \quad (1)$$

where x is the cross-shore coordinate directed positive offshore, $F_x = F \cos \theta$ is the shore-normal component of wave energy flux F per unit surface width, θ is the angle of wave crests to a baseline (y axis) running alongshore, κ is an empirical breaking-wave decay coefficient (found by D3 to equal 0.15), $d = h + \eta$ is the total water depth as the sum of the still-water depth h and the mean displacement η of the water surface (setdown and setup) from the still-water level, and F_s is the energy flux of a stable wave defined by D3 (flux of a broken wave at a depth where it ceases breaking and reforms). The wave direction is determined by Snell's law, $d(\sin \theta/C)/dx = 0$. Wave-current interactions have been shown to be negligible for a one-dimensional longshore-current model [Dalrymple, 1980; Thornton and Guza, 1986; KL].

The energy flux is $F = EC_g$, where $E = \rho g H^2/8$ is the wave energy density per unit surface area, in which ρ is the density of water, g is the acceleration due to gravity, and H is the wave height. The wave group speed $C_g = CN$, where $C = L/T$ is the wave celerity (L is the local wavelength, and T is the wave period), and $N = [1 + (4\pi d/L)/\sinh(4\pi d/L)]/2$. The wave energy flux for a stable wave appearing in (1) was defined by D3 as $F_s = E_s C_g$, in which the energy E_s of a wave that has stabilized or reformed is expressed in terms of a stable wave height defined as $H_s = \Gamma d$, in which Γ is an empirical coefficient found by D3 to have a value of about 0.4.

Wave calculations proceed by a forward-difference numerical solution scheme from the seaward end of the numerical grid, located well seaward of the point of wave breaking, until the first breakpoint is detected; if breaking is initiated (through the depth-limiting criterion $H = \gamma_b d$, where γ_b is the breaker index ≈ 0.78 for individual waves), the wave decay coefficient κ in (1) is assigned the value 0.15, and energy dissipation takes place. If breaking has occurred, a check is made for the possibility of wave reformation, that is, if the calculated wave energy flux has fallen below the

stable energy flux; at that point, κ is reset to zero. An arbitrary number of breakpoints with intermediate zones of wave reformation can be described.

For simulating field conditions, wave height and angle are calculated for individual waves, either selected randomly from a Rayleigh distribution of heights defined at the seaward end of the grid [LK] or as specified from a time series record. The production of turbulence per unit surface area P is obtained at each grid point for each individual wave as

$$P = dF_x/dx \quad (2)$$

An average turbulent energy production is then calculated at each grid point for all the waves, typically 100 or more, randomly selected to form the ensemble. This calculation procedure has replicated measured non-Rayleigh wave height distributions in the surf zone that deviate from the Rayleigh distribution because of depth-limited wave breaking over an irregular bottom (KL, LK; see *Dally* [1990] for similar independent verification of the individual wave procedure applied to random waves). A monochromatic wave condition such as that produced in the laboratory is directly simulated by input of a single wave height and angle (omitting the random selection procedure) from which the turbulent energy production of the constant wave condition is obtained. An alternative to the individual-wave approach for random waves has been given by *Thornton and Guza* [1983], who applied an empirical weighting function giving the fraction of waves breaking in a Rayleigh distribution that is assumed to exist at each calculation point across shore. The individual-wave approach does not rely on an assumed wave height distribution in the surf zone, providing the distribution as a product, and it can model monochromatic wave breaking, which the empirical weighting method cannot.

Turbulent Kinetic Energy Transport Equation

In general, the longshore current is calculated under the assumption that the driving forces are given by the gradients in radiation stress; that is, as the waves break and create turbulence, the decrease in wave momentum flux is instantaneously balanced by a shear stress due to the generated longshore current. However, as pointed out by *Roelvink and Stive* [1989], a distinction should be made between the loss of organized wave energy and the dissipation of TKE when determining nearshore currents and changes in mean water level. Wave-induced turbulence contributes to the onshore transport of momentum, implying that decay in radiation stress does not correspond to immediate dissipation by viscous forces and that a shift in time and space occurs owing to the transport of TKE [Svendsen, 1987]. In transport models for the TKE, the energy dissipation D is parameterized as [Rodi, 1980]

$$D = \rho c_D \frac{k^{3/2}}{l} \quad (3)$$

where c_D is an empirical constant discussed below; k is the TKE per unit mass, taken here to be a time and depth average; and l is a representative length scale associated with the larger eddies that are most effective in transporting and dissipating the TKE.

Svendsen [1987] showed on the basis of laboratory measurements that a small portion (2–6%) of the energy in the

breaker is dissipated below trough level, also indicating that the vertical variation in the time mean of k below trough level is small. Thus most of the transport of turbulent momentum takes place above trough level. A natural approach for describing the macrofeatures of wave breaking, including the transport of momentum, is to schematize the water column into two layers, with one layer extending from the bottom up to trough level and another layer above trough level with a thickness equal to the wave height. Similar schematizations have previously been employed for calculating macrofeatures of surf zone hydrodynamics [Stive and Wind, 1986; Thieke and Sobey, 1990].

Limited data exist regarding the characteristics of turbulence in the surf zone, particularly above trough level, where turbulence measurements are performed with great practical difficulty owing to the air-water mixture and the strong intermittency of the turbulence in this region. Nadaoka [1986] studied surf zone flows including turbulence in the "upper layer" (above trough level) and concluded that violent mixing of momentum takes place in this layer. Furthermore, by observing the movement of neutrally buoyant beads, he found that the advection speed in the upper layer was much greater than in the lower layer (below trough level).

Measurements below trough level clearly show that the turbulence intensity increases from near zero just outside the breakpoint (point of maximum height of shoaling waves) of monochromatic waves to a maximum located somewhat shoreward of the break point [Svendsen, 1987]. Time-averaged turbulent conditions below trough level should reflect the spatial distribution of k above trough level, implying that the cross-shore distribution of k and the shift in dissipation are similar above and below trough level. The spatial lag between production and dissipation of TKE causes a shift in the momentum decay, because wave momentum is temporarily stored as turbulent momentum. The spatial lag must be represented for accurate longshore current modeling and is a central feature of the model introduced here.

The cross-shore distribution of the mean TKE above trough level, with a thickness assumed to be the wave height, is calculated in the present study through a general steady state transport equation [compare McGuirk and Rodi, 1978; Rastogi and Rodi, 1978; Rodi, 1980]

$$\frac{d}{dx} \left(\nu_t H \frac{dk}{dx} \right) + \frac{d}{dx} (kCH \cos \theta) + \frac{P}{\rho} - c_D k^{3/2} = 0 \quad (4)$$

where ν_t is the kinematic eddy viscosity. In random wave modeling, the root-mean-square (rms) wave height is used as the thickness of the above-trough layer. The first term in (4) describes diffusion of TKE, for which the kinematic eddy viscosity is parameterized as [Rodi, 1980]

$$\nu_t = c_\mu k^{1/2} l \quad (5)$$

where c_μ is an empirical coefficient, and the length scale l of the turbulent eddies is of the order of the water depth or wave height in shallow water. The second term represents the advection of TKE with a speed equal to the local wave celerity (note that the advective speed is taken as negative or onshore in (4), since the TKE is advected in a direction opposite the positive x axis). The last term in (4) is the energy dissipation integrated over the above-trough layer under the assumption of k independent of the vertical

coordinate. The physical picture of a TKE uniform in the layer above trough level is intuitively reasonable for a well-mixed surf [cf. Nadaoka, 1986]. Equation (4) differs from previous TKE transport equations used in nearshore wave and current modeling [Roelvink and Stive, 1989; Nairn et al., 1990] by inclusion of the horizontal diffusion term that is standard in turbulence modeling and by employing the transport equation for the region above trough level. Implicitly, in time averaging of k , those time intervals when a point is not submerged are excluded [Thieke and Sobey, 1990]. In turbulence modeling, the generally accepted value for the empirical coefficients is $c_\mu c_D = 0.08$ [Launder and Spalding, 1972; Rodi, 1980], and this value was also employed in the present study.

Before (4) can be solved to yield the mean TKE in the upper layer, the turbulent length scale l has to be specified, which is typically done by establishing an empirical relationship [Rodi, 1980]. The length scale depends on the type of turbulent flow and is expected to vary according to the local flow characteristics. With knowledge of surf zone turbulence presently limited, especially for the region above trough level, use of a simple representative value for the length scale is necessary. Svendsen [1987] estimated l below trough level to be 20–30% of the water depth based on undertow measurements [cf. Deigaard et al., 1991]. The length scale above trough level should also be of the order of the water depth or the local wave height. In the present study, l was set equal to the root-mean-square wave height H_{rms} , and $c_\mu = 0.5$, which gives a length scale comparable to values reported by Svendsen [1987]. If $c_\mu = 0.5$, then $c_D = 0.16$, following the guidance of Rodi [1980], which requires $c_\mu c_D = 0.08$.

Equation (4), with the advective term represented by an upwind difference, is solved by a double-sweep method analogous to that used by LK for the longshore current velocity. The numerical solution scheme was tested for the presence of numerical dissipation by varying the grid step size; no discernible artificial dissipation was detected for any practical range of cell sizes used in the longshore current modeling. Formulation of the shoreward boundary condition is of most significance, whereas at the seaward boundary the solution is less sensitive to the particular choice of boundary condition. Several different conditions were evaluated at the shoreward boundary, including no transport, diffusion only, and advection only of TKE across this boundary. If the condition of no transport of TKE across the shoreward boundary is imposed, TKE will be conserved in the surf zone, whereas the other two boundary conditions allow leakage of TKE into the wetted area shoreward of the last wave calculation point, taken to be the nominal swash zone. In the results presented here, the shoreward boundary condition $dk/dx = 0$ was selected, allowing advection of TKE into the swash zone. Such a condition was considered to give the most realistic description of the hydrodynamics near shore. Leakage of TKE results in the condition $D \leq P$ in the calculation domain. At the seaward boundary a condition of $k = 0$ was employed.

Longshore Current and Setup Model

Under the stated assumptions, the vertically integrated, time-averaged momentum equations for nearshore water motion [Mei, 1983] are

$$g \frac{d\eta}{dx} = -\frac{1}{\rho d} \frac{dS_{xx}}{dx} - \frac{\rho_a C_w}{\rho d} |W|W \cos \phi \quad (6)$$

for the cross-shore (x) component, and

$$\frac{d}{dx} \left(\varepsilon_L d \frac{dV}{dx} \right) - f_{by} = \frac{1}{\rho} \frac{dS_{xy}}{dx} - \frac{\rho_a C_w}{\rho} |W|W \sin \phi \quad (7)$$

for the longshore (y) component. In these equations, S_{xx} and S_{xy} are excess momentum flux tensors (defined below), ρ_a is the density of air, C_w is a wind drag coefficient, W is the wind speed at 10-m elevation, ϕ is the wind direction defined as positive directed onshore, ε_L is a kinematic eddy viscosity coefficient controlling lateral diffusion of momentum below trough level, and f_{by} is related to the bottom friction stress (described below). The wind drag coefficient given by the *WAMDI Group* [1988], derived from measurements made in intermediate-depth water, is adopted.

The excess momentum flux tensors each consist of two parts, one a contribution from the transport of wave momentum (radiation stress) and another from the transport of turbulent momentum above trough level (Reynolds stress). If the two contributions are uncorrelated, they may be separated according to

$$\begin{aligned} S_{xx} &= S_{xx}^w + S_{xx}^t \\ S_{xy} &= S_{xy}^w + S_{xy}^t \end{aligned} \quad (8)$$

where the superscripts w and t refer to wave and turbulence, respectively. In the present model, S_{xx}^w and S_{xy}^w are specified by *Longuet-Higgins and Stewart* [1964], and S_{xx}^t and S_{xy}^t are parameterized using the TKE. Also, it is assumed that the turbulent momentum transport above trough level is dominant, and only this region is modeled in detail through the TKE transport equation. The turbulent momentum exchange below trough level is schematically described through a mixing term in (7).

The radiation stress component S_{xx}^w for the organized wave motion calculated from linear theory is given by

$$S_{xx}^w = E[N (\cos^2 \theta + 1) - \frac{1}{2}] \quad (9)$$

and the component S_{xy}^w is given by

$$S_{xy}^w = \frac{1}{2} NE \sin(2\theta) \quad (10)$$

Expressions for the turbulent momentum transport may be determined in a manner similar to the procedure for deriving S_{xx}^w and S_{xy}^w for waves obliquely incident on a beach [*Longuet-Higgins and Stewart*, 1964; *Mei*, 1983]. Thus in a coordinate system traveling with the waves (unrotated system), the following parameterization is made for describing the turbulent momentum transport S_{xxu}^t and S_{yyu}^t , respectively,

$$\begin{aligned} S_{xxu}^t &= \int_H \rho (\overline{u_t^2} - \overline{w_t^2}) dz = \beta_1 \rho k H \\ S_{yyu}^t &= \int_H \rho (\overline{v_t^2} - \overline{w_t^2}) dz = \beta_2 \rho k H \end{aligned} \quad (11)$$

where u_t , v_t , and w_t are the turbulent velocity fluctuations in x , y , and z directions of the unrotated coordinate system,

respectively; β_1 and β_2 are empirical coefficients that depend on the turbulence characteristics of the flow in the above-trough layer of assumed thickness H ; and an overbar denotes time averaging. In a general development, the turbulent momentum transport contains a cross-term S_{xyu}^t that depends on the covariance $u_t v_t$. Assuming as before that the wave and turbulent motions are uncorrelated,

$$S_{xyu}^t = \int_H \rho \overline{u_t v_t} dz \quad (12)$$

Estimation of this contribution to the momentum transport is more difficult than for the terms in (11), although a similar parameterization could be introduced, requiring another empirical coefficient in the model.

To derive expressions for the Reynolds stresses for waves arriving at an oblique angle, a tensor transformation is carried out to yield the turbulent driving terms in (6) and (7)

$$S_{xx}^t = \rho k H (\beta_1 \cos^2 \theta + \beta_2 \sin^2 \theta) + 2S_{xyu}^t \sin \theta \cos \theta \quad (13)$$

$$S_{xy}^t = \rho k H (\beta_2 - \beta_1) \sin \theta \cos \theta + S_{xyu}^t (\cos^2 \theta - \sin^2 \theta) \quad (14)$$

The values of the coefficients β_1 and β_2 depend mainly on the degree of isotropy of the turbulent flow above trough level, that is, the relationship between the turbulent intensities in the respective coordinate directions. In the case of turbulence above trough level induced by breaking waves, the turbulent intensities in the two coordinate directions perpendicular to the wave propagation (v_t and w_t) should be of about the same magnitude [cf. *Svendensen*, 1987], implying that $\beta_2 = 0$. Assignment of an appropriate value to β_1 is more difficult, but analogies with other turbulent flows indicate values in the range 0.2–0.8 [*Townsend*, 1976; *Svendensen*, 1987]. However, because few turbulence measurements exist above trough level, β_1 must be determined primarily on the basis of comparison with measurements of derived quantities such as the longshore current and setup.

To completely specify the turbulent momentum transport, the cross-term S_{xyu}^t has to be estimated, which is difficult because of the lack of relevant turbulence measurements of the covariance $u_t v_t$. *Townsend* [1976] presents values of the covariance between turbulent fluctuations in two perpendicular directions normalized with TKE in the interval 0.15–0.30. However, these values refer to turbulent flows where u_t is in the direction of the flow that generates the turbulence and v_t is perpendicular to this flow in the dimension of the minimum flow thickness (depth). In the present case, the covariance $u_t v_t$ involves the turbulent fluctuations in the horizontal plane, with v_t taken in the direction perpendicular to the flow that does not correspond to the minimum flow thickness. A greater flow thickness will in general imply a smaller $u_t v_t$ term, because this momentum exchange will be characterized by a larger length scale. Thus it is expected that the covariance values reported by *Townsend* [1976] represent an upper limit if applied to estimate the S_{xyu}^t term.

Generally, in longshore current modeling, the $u_t v_t$ covariance is set proportional to the shear in the longshore current which diffuses momentum seaward and shoreward of the peak in the longshore current [*Mei*, 1983]. If the lateral mixing strength above and below trough level is similar, then S_{xyu}^t is at least an order of magnitude smaller than $\rho k H$ in

(13) and (14), and the S'_{xyu} term in (13) is negligible. For small wave angles, the trigonometric functions in (14) reduce the first term by an order of magnitude relative to the S'_{xyu} term, potentially making both terms similar in magnitude. Because the magnitude and sign of S'_{xyu} are unknown and because this term would contribute only in the sense of increasing mixing (diffusing momentum, but not shifting the peak) which is accounted for in the lower layer, this term is neglected in the remainder of this paper.

In all simulations presented in this paper, $\beta_1 = 1.0$ and $\beta_2 = 0.0$ were used for calculating the Reynolds stresses. The value $\beta_1 = 1.0$ was chosen because it gives a near balance between the gradients in the radiation stress and Reynolds stress in the incipient breaking zone. Low values of β_1 , such as 0.22 used by *Roelvink and Stive* [1989] for modeling the transport of TKE below trough level, failed to produce the observed flat cross-shore distribution of the longshore current. *Nairn et al.* [1990] also noted the need for a large value of β_1 to obtain realistic modeling results for breaker-induced currents and water level change.

Equation (6) governs the mean water surface displacement η , and (7) gives the longshore current V , for which the driving forces are given by (9), (10), (13), and (14). The eddy viscosity coefficient ε_L , which parameterizes the lateral mixing below trough level, is expressed according to the empirical formulation by KL and LK as

$$\varepsilon_L = \Lambda u_m H \quad (15)$$

in which Λ is an empirical coefficient representing the lateral mixing strength, and $u_m = gHT/[2L \cosh(2\pi d/L)]$ is the amplitude of the horizontal component of the wave orbital velocity at the bottom. In deep water, ε_L goes to zero as u_m gradually goes to zero, with a corresponding gradual decay in the eddy viscosity. *Battjes* [1975] suggested that water depth is the appropriate length scale of lateral mixing on uniformly sloping beaches, and local wave height is a reasonable generalization of this concept for barred beaches. *Putrevu and Svendsen* [1991] showed that the high tail in eddy viscosity long known to be necessary for longshore current modeling (compare the review by KL) is produced by momentum carried by the undertow. Equation (15) must then be viewed as representing an effective eddy viscosity; however, the predicted shape of the longshore current profile depends mainly on the magnitude of the eddy viscosity and is relatively insensitive to the chosen form [*Kraus et al.*, 1980].

The second term on the left side of (7) represents the longshore component of the bottom friction stress, the major retarding force for the longshore current, and is expressed by a quadratic law in the total fluid velocity as

$$f_{by} = c_f \langle (u_m^2 \cos^2 \tau + V^2 + 2u_m V \cos \tau \sin \theta)^{1/2} \cdot (V + u_m \cos \tau \sin \theta) \rangle \quad (16)$$

in which c_f is a bottom friction coefficient; $\tau = 2\pi t/T$, where t denotes time; $u_m \cos \tau \sin \theta$ is the longshore component of the wave orbital velocity at the bottom; and triangular brackets denote time averaging over a wave period.

In evaluation of (16), the closed-form approximation of *Nishimura* [1982, 1988] is used to explicitly calculate the time average [LK], but iteration is still required because of the quadratic dependence in V . *Thornton and Guza* [1986]

and LK examined differences in longshore current model predictions using the full quadratic friction term (16) and the more common linearized versions [e.g., *Bowen*, 1969; *Longuet-Higgins*, 1970a, b]. They found that the value of the friction coefficient c_f associated with a linear friction law (weak longshore current magnitude compared with that of the horizontal wave orbital velocity) can be on the order of 30 to 50% greater for fitting measured current profiles on uniformly or nearly uniformly sloping bottoms than that associated with the quadratic law for comparable fit. Because the quadratic friction law is the more general and theoretically correct representation, it is used in the present model.

In longshore current modeling, the value of the friction coefficient is employed as the main fitting parameter. We devoted considerable effort to examining current profile predictions obtained from three forms of c_f : a constant, empirically determined value (the most typical choice in longshore current modeling); the wave friction coefficient of *Jonsson* [1966] as first used by *Thornton* [1970] and followed by a few authors; and the Manning friction coefficient, first used by *James* [1974]. Our comparisons to field and laboratory data indicated that the Manning friction coefficient gave best agreement near the shoreline and in the vicinity of the current peak in the trough of the beach profile. The Manning friction coefficient is

$$c_f = g(n^2/d^{1/3}) \quad (17)$$

in which n is the empirically determined dimensional ($s m^{-1/3}$) Manning resistance coefficient. For turbulent flow, as occurs in the surf zone, n is approximately constant but is still a function of bottom roughness. In the formulation of (17), the hydraulic radius of open-channel flow was taken as the total water depth, corresponding to a wide channel, following standard practice in tidal-flow and similar long-wave calculations.

In application of the five-equation model to a field situation, a Rayleigh distribution of wave height based on a given rms wave height and fixed wave angle and period are input to the wave model on a wave-by-wave basis. The spectral peak period and mean direction are used, implying a narrow-band, single-peak spectrum. Turbulent-energy production values associated with each wave are averaged to obtain an ensemble mean production across the surf zone. The ensemble production is input to the TKE transport equation to solve for a mean k in the above-trough layer, from which the Reynolds stresses in the momentum equations are determined. The solution process is coupled between the mean water level calculation (6) and the wave energy balance equation (1), and five iterations are typically required to achieve convergence to less than 1% change in η anywhere on the grid. In the iteration, the same individual waves are selected in a Monte Carlo process from the Rayleigh distribution. This iterative procedure is equivalent to simultaneous solution of the wave transformation, mean water level, and longshore current as an ensemble average, typically calculated from 100 or more individual waves.

The numerical solution scheme for calculating the wave height, wave angle, mean water level, and longshore current velocity at evenly spaced points across the surf zone has been described in KL and LK. The velocity and TKE are calculated at grid cell locations that alternate with wave-related quantities in a staggered finite-difference scheme.

TABLE 1. Input Wave, Wind, and Tide Level Data

Time	H_{rms} , m	T , s	θ ,* deg	Tide, m	W , m/s	ϕ ,* deg
0100	0.94	9.7	32.0	0.2	3.3	152.7
0400	0.82	10.7	12.0	0.3	3.4	-169.2
0700	0.68	9.7	32.0	-0.3	3.3	-144.5
1000	0.71	9.7	34.0	-0.4	3.0	-71.8
1300	0.65	9.7	22.0	0.2	3.2	-24.0
1600	0.74	10.7	18.0	0.3	3.1	21.4
1900	0.83	12.0	18.0	-0.2	4.9	50.6
2200	0.79	12.0	18.0	-0.5	6.6	149.7

*Defined as clockwise from shore normal.

The wave height is solved by forward differencing, and the velocity is solved by an efficient and highly stable implicit double-sweep scheme. Specification of the seaward boundary condition in the alongshore momentum equation is straightforward: zero wave-induced current velocity at the end of the grid, that is, only a wind-induced current if a wind is imposed. At the shoreward-most cell, an explicit calculation without lateral mixing is performed to give the boundary current velocity.

CALCULATION RESULTS

DELILAH Data

Root-mean-square wave height, mean longshore current velocity, and mean wave setup were calculated for the October 14 DELILAH data. The input mean wave direction and peak wave period were taken from the 8-m array for eight cases corresponding to the eight collection times at the array. The input rms wave height was taken from the most seaward of the nine nearshore pressure gages, and the height was inversely refracted and shoaled to the 8-m depth. Input of the rms height measured at the 8-m array caused a 15% overprediction of the wave height at the most seaward pressure gage that may be attributable to the use of linear refraction and shoaling in the model. The model grid consisted of 380 cross-shore cells with a spacing of 1 m. The wave model parameters ($\gamma_b = 0.78$, $\Gamma = 0.4$, and $\kappa = 0.15$) and the turbulence coefficient values of $c_\mu = 0.5$ and $c_D = 0.16$ were used for all eight cases, as was discussed previously. The mixing strength parameter Λ was set at 1.0 in initial calculations as a representative value, and the main fitting parameter was taken to be the Manning n , which was determined as 0.020 to give an optimal fit for all cases. The value 0.020 is in the range of values normally assigned to open-channel flow on "clean, recently completed excavated or dredged earth" [Chow, 1959].

One hundred individual waves were randomly selected from a Rayleigh wave height distribution defined by the measured rms height to simulate the wave field. The nearshore wave and current measurements were averaged over the 2-hour interval concurrent with the 8-m array measurements. Input wind speed, wind direction, and tide elevation were averaged over the same interval. The input wave, wind, and tide data are given in Table 1. The wave field changed slowly through time, with the greatest nearshore variation caused by tide.

The five-equation model results for the eight cases on October 14 are given in Figure 4. The figure shows the water

depth along the profile (adjusted for the tide), the measured and calculated rms wave height, the measured and calculated mean longshore current, and the calculated mean water surface elevation. Results from the four-equation model (Manning $n = 0.027$) for the same cases are shown in Figure 5. The improvement in current prediction of the five-equation model over the four-equation model is striking. The wave transformations calculated with the two models are nearly the same, with small differences due to differences in the calculated mean water surface elevation. The distribution of the longshore current from the four-equation model consists of two distinct peaks, at the bar and at the steep foreshore, centered at the points of maximum wave height decay. The distribution of the longshore current from the modified or five-equation model is given as a broad, flat peak in the velocity in the bar trough, with a second peak on the foreshore. Sensitivity tests with wind speed and direction indicated that wind was not a significant factor in predictions of either model.

The improved performance of the five-equation model over the four-equation model is understood by examination of turbulence production P and dissipation D , illustrated in Figure 6 for the DELILAH case 0100 hours. The calculated production exhibits two sharp peaks, with effectively zero production of turbulent energy in the trough (region between approximately 140 and 180 m) where waves reform. The TKE transport equation (4) advects the turbulent energy from points of incipient breaking of individual waves and shifts it into the trough. The shoreward shift of turbulent energy is essential for describing the observed persistent, high-magnitude current in the trough. The calculated TKE dissipation is relatively evenly distributed through the surf zone except for a peak at the steep shore face and swash regions, where intense wave breaking occurs. It is not clear whether the peak in the TKE and current near the shoreline exist in the field as universally as predicted by the model. Model assumptions begin to break down in the swash zone owing to strong nonlinear wave interactions and probable dominance of beach permeability in controlling fluid flow. Approximately 30% of the TKE was transported across the shoreward boundary for the DELILAH simulations. Gradients in the radiation stress and Reynolds stress are shown in Figure 7. The two components approximately balance in the outer breaker zone, so the total forcing is small in that region. The wave component dominates shortly after breaking, and the turbulent component dominates further into the trough. The forcing for the four-equation model is equivalent to that from only the radiation stress shown in Figure 7.

Figure 8 compares the bottom friction coefficient calculated by the Jonsson [1966] formula with the roughness element (grain size) adjusted to give a best fit (grain-size diameter of 0.025 mm, an unrealistically small grain size) and the friction coefficient from the Manning formula (17) for case 0100 hours. Both formulae produce the same order of magnitude and general behavior across the profile except near the shoreline, where the Manning friction coefficient rises sharply because of its depth dependence (a similar trend is noted over the bar, at 200 to 250 m, where the Manning friction coefficient increases slightly, whereas the Jonsson friction coefficient decreases). For surf zones in the field, the Reynolds number typically far exceeds the empirical range from which the Jonsson friction coefficient was developed.

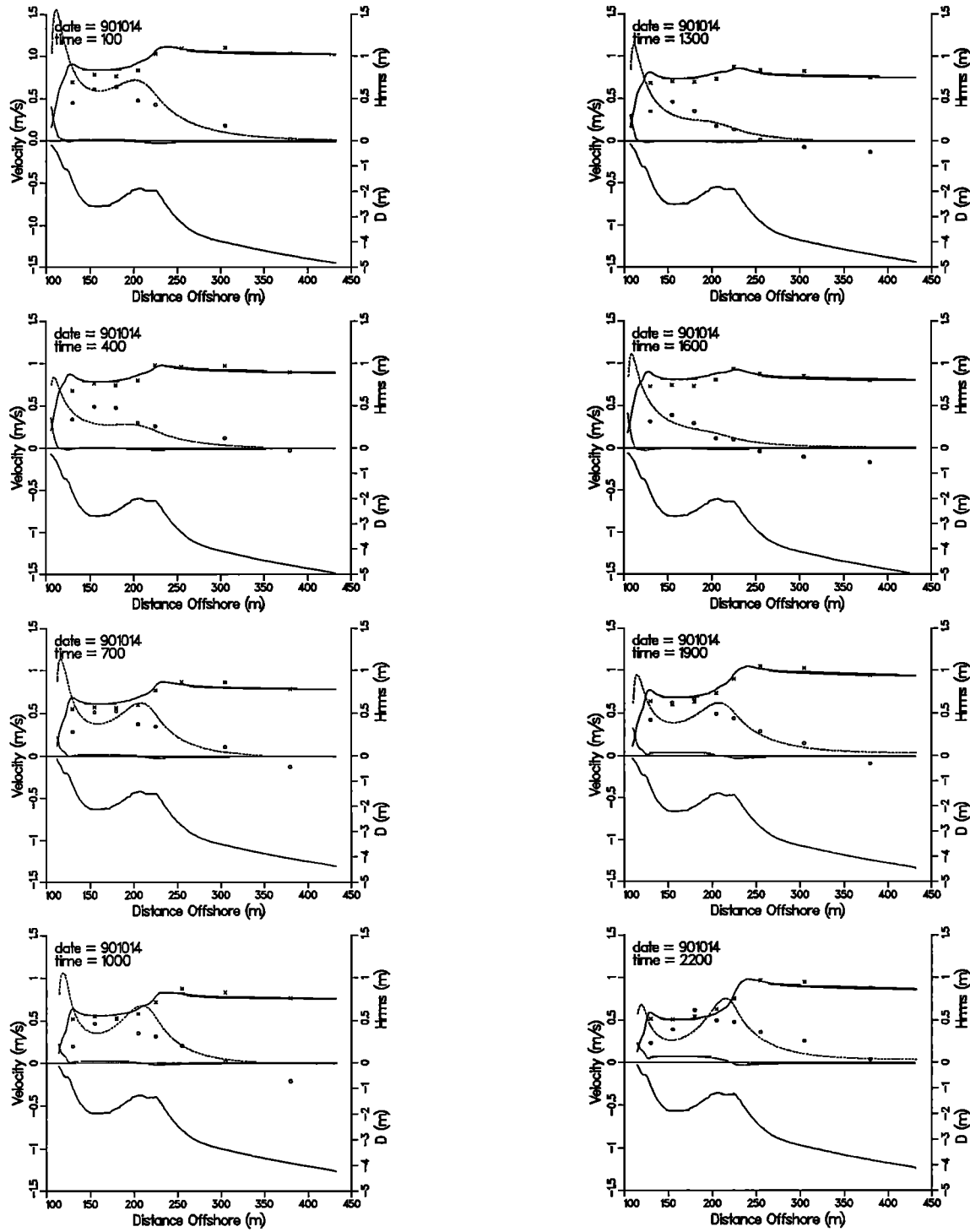


Fig. 4. Comparison of five-equation model wave transformation (solid curves), longshore current (dashed curves), and mean water level (chain-dot curves) calculations to DELILAH field data.

A least squares error E_v provides an objective measure of goodness of fit of calculated and measured longshore current:

$$E_v = \left(\frac{\sum (V_{\text{meas}} - V_{\text{calc}})^2}{\sum (V_{\text{meas}})^2} \right)^{1/2} \quad (18)$$

An error in prediction of the wave height was calculated similarly.

Wave height transformation. The average least squares error in the wave height prediction was 8.0%, ranging between 5.1 and 9.4% for the eight cases, as summarized in Table 2. The model tended to overpredict the measurements in the trough, but overall the model predicts the wave height well with default values recommended by its developers [D3].

Longshore current. The average least squares error in the longshore current results was 55.9%, ranging between

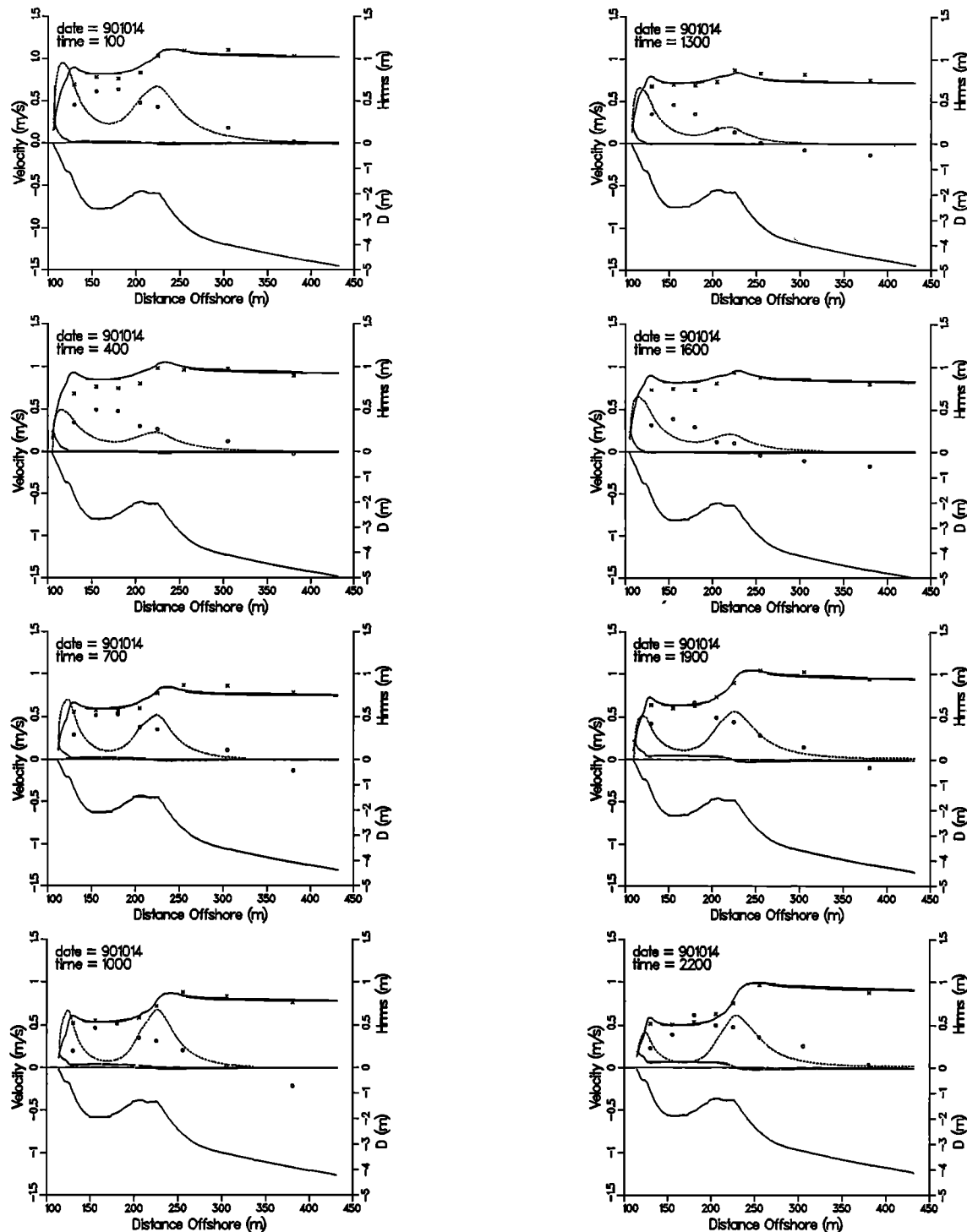


Fig. 5. Comparison of four-equation model wave transformation (solid curves), longshore current (dashed curves), and mean water elevation (chain-dot curves) calculations to DELILAH field data.

36.0 and 90.2% for the eight cases (Table 2). The average least squares error for the four-equation model was 67.2%. The greatest error tended to occur for cases with the maximum tide elevations (cases 0400, 1300, and 1600). The larger errors at these times may be the result of adding a constant tide elevation at each cross-shore grid point and overestimating the depth at the nearshore points. The model also consistently overpredicts the velocity at the most shoreward gage (error of 125%).

Sensitivity Tests

The values of the empirical parameters β_1 and Λ , which respectively determine the strength of the turbulent momentum transport in the above-trough level ((13) and (14)) and lateral mixing in the below-trough level (15), influence the shape of the cross-shore distribution of the longshore current. The degree of influence was investigated in sensitivity tests, as shown in Figures 9 and 10 for the measurements of

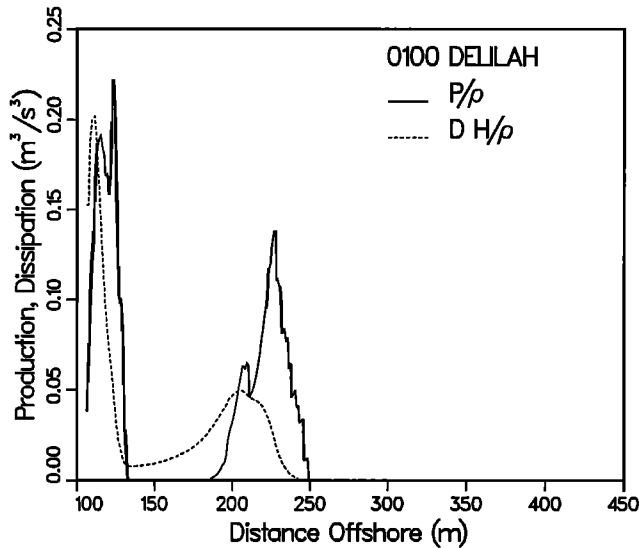


Fig. 6. Calculated wave turbulence production P and dissipation D across the beach profile (DELILAH 0100 hours).

0100. Decrease of β_1 from the assigned value of 1.0 to 0.2, as shown in Figure 9, moves the peaks in the current offshore while increasing their magnitude, reduces the shoreward peak slightly, and produces a slight decrease in the current on the shoreward side of the bar. Larger values of β_1 increase the spatial shift between production and dissipation of TKE by increasing the storage term in (4).

A decrease in Λ from the assigned value of 1.0 to 0.1, as shown in Figure 10, increases the magnitudes of the two peaks in the current and decreases the current in the trough, moving the minimum in the trough shoreward. This result is expected on the basis of similar tests of the strength of mixing [Longuet-Higgins, 1970b; LK].

The tests indicate that model predictions are not greatly sensitive to a reasonable variation in magnitudes of the coefficients β_1 and Λ , meaning that another choice of, say,

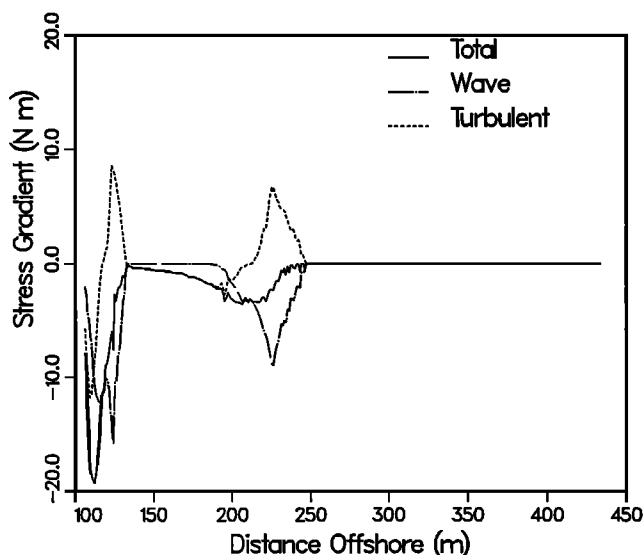


Fig. 7. Gradient in total, radiation, and Reynolds stress across the beach profile (DELILAH 0100 hours).

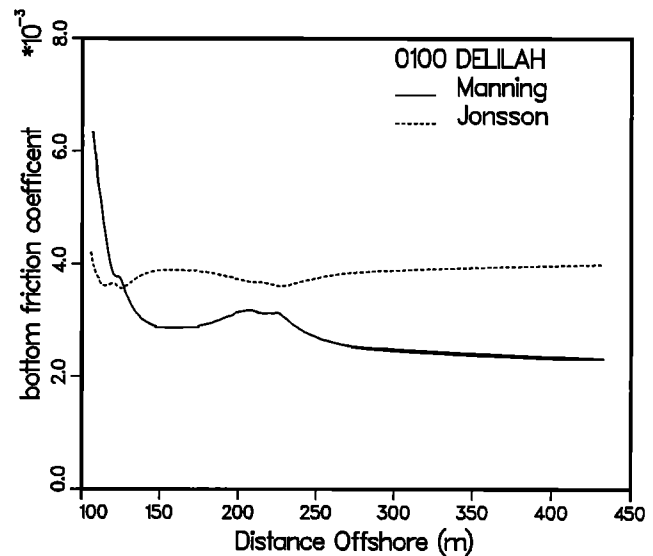


Fig. 8. Calculated *Jonsson* [1966] friction coefficient and Manning friction coefficient (DELILAH 0100 hours).

10 or 20% change in value would not greatly change the character of the computed result.

In closing discussion of the sensitivity of the model to empirical parameters, we mention that tests showed that for the field and laboratory cases examined in this paper, the TKE diffusion term in (4) had negligible effect on the longshore current profile. It does enter in the shoreward boundary condition, however, because of the steep gradient in the TKE.

Visser Laboratory Data

Visser [1982, 1984, 1991] measured the longshore current velocity and change in water surface elevation generated by monochromatic waves on a uniformly sloping beach in a laboratory facility carefully designed to minimize basin effects such as reflection and artificial circulation. Comparisons for four of the seven Visser cases selected for modeling by LK are presented here to show the effect of including the TKE transport equation for monochromatic waves (single-wave input, no ensemble average). Visser cases 1, 3, 4, and 7 were those with largest wave angle, largest wave height, and smooth and rough bottoms for the same offshore (model input) wave conditions, respectively (Table 3). Also, the setup and setdown measurements were made under highly controlled conditions in the laboratory to allow checking of the mean water surface calculation that are not possible with field measurements.

For these calculations the same empirical parameters as in the DELILAH cases were used in the wave model, TKE transport equation, and longshore current model except that γ_b was set to the measured value (0.74 to 1.0) and in both the four- and five-equation models the mixing strength parameter was set to $\Lambda = 0.15$, which is lower than the field-determined value but similar to the relative magnitudes found by LK; model predictions were insensitive to small changes in Λ , and no refined optimization with this parameter was made. The friction coefficient was the main fitting parameter for the five-equation model, and the optimal average Manning n was determined to be 0.015 for the

TABLE 2. Least Squares Error in H_{rms} and V Predictions for DELILAH Data

	Time							
	0100	0400	0700	1000	1300	1600	1900	2200
$H_{rms}, \%$	8.9	9.4	6.5	5.1	6.8	8.9	6.9	9.1
$V, \%$	54.3	36.0	69.2	90.2	55.0	65.8	37.0	47.9
Total								

smooth bottom (cases 1, 3, and 4) and 0.023 for the rough bottom (case 7). These values of Manning n agree with design values compiled for open-channel flow over smooth and rough concrete surfaces, respectively [Chow, 1959].

Comparisons of measured versus calculated wave height, longshore current, and setup are given in Figure 11. Similar comparisons for the four-equation model are given in Figure 12, for which $n = 0.016$ and 0.026 for the smooth and rough bottom cases, respectively. Figures 11 and 12 show that the peak in the current distribution is better predicted by the five-equation model, as are the overall shapes of the distributions.

Because the input wave conditions and slope varied greatly between the cases, the least squares error, listed in Table 4, was calculated for each case separately to avoid skewing the results toward the cases with higher heights and velocities. The least squares error in wave height ranged from 8.7 to 35.6%, compared with 9.0 to 36.7% for the four-equation model; the error in longshore velocity ranged from 13.0 to 20.5%, compared with 27.9 to 48.5% for the four-equation model; and the error in water surface elevation ranged from 32.3 to 59.4%, compared with 12.4 to 40.6% for the four-equation model. The errors in the five-equation model for predicting the longshore current were approximately half of those calculated for the four-equation model.

Errors in calculated mean water surface elevation were larger for the five-equation model. However, the five-equation model gave improved qualitative agreement between calculated and measured mean water surface elevations in reproducing the smooth transition from point of setdown to start of setup, location of maximum setdown, and flatness in the region of setdown. This smooth transition

from setdown to setup is obtained even for monochromatic waves through the smoothing action of the TKE transport equation. Improved agreement in mean water surface elevation could be obtained by tuning the wave transformation model, in particular by adjustment to reproduce the location of the measured point of wave breaking.

CONCLUDING DISCUSSION

Measurements of the longshore current over the barred profile at Duck, North Carolina, showed a broad peak in the current distribution over the longshore trough that would be considered anomalous in traditional mathematical models of the current that compute the driving force only from wave height decay. Following and generalizing work by Roelvink and Stive [1989], a TKE equation was introduced to compute the cross-shore distribution of TKE from the turbulence production by wave breaking. Reynolds stress components associated with turbulent momentum were expressed in terms of the TKE. Use of this model, termed a "five-equation" model by the addition of the turbulent energy transport equation to the traditional model, gave improved agreement (20–50% reduction in least squares error) with the measured time average longshore current distribution over the barred-bottom field beach profile. The model also gave quantitatively improved agreement with high-quality laboratory data of the longshore current and qualitatively improved agreement for the associated mean water surface elevation generated by monochromatic waves obliquely incident to a uniformly sloping beach. In the comparisons to field and laboratory measurements, the key factor in achieving improved agreement with the measurements was the shore-

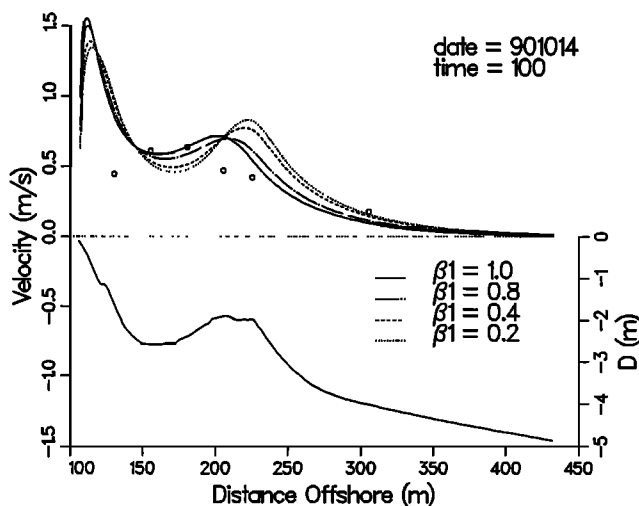


Fig. 9. Sensitivity tests of β_1 with the calibrated model (DELILAH 0100 hours).

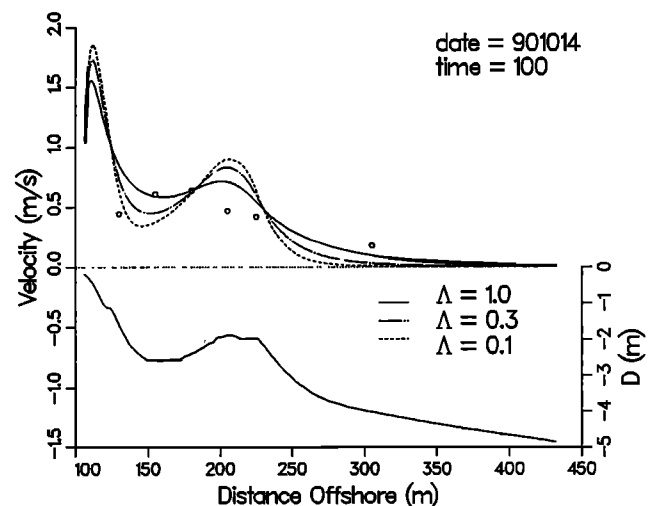


Fig. 10. Sensitivity tests of Λ with the calibrated model (DELILAH 0100 hours).

TABLE 3. Visser Input Data

Case	H , m	T , s	θ , deg	Beach Slope	$(\gamma_b)_{\text{meas}}$
1	0.072	2.0	31.1	0.101	1.00
3	0.089	1.0	15.4	0.101	0.85
4	0.078	1.0	15.4	0.050 (smooth)	0.83
7	0.078	1.0	15.4	0.050 (rough)	0.74

TABLE 4. Least Squares Error in H and V Predictions for Visser Data

	Case			
	1	3	4	7
H , %	8.7	11.9	10.0	35.6
η , %	48.0	59.4	32.3	...
V , %	16.8	13.0	18.9	20.5

*Not measured.

ward shift and smoothing of the energy dissipation provided by the turbulent kinetic energy transport equation.

The driving force for the (random wave) field comparisons was computed from an ensemble average of the turbulence production contributed from individual waves. The individual wave model does not depend on assumed forms for the wave height distribution in the surf zone, providing such distributions as part of the calculation [KL; LK], and it also allows ready calculation for laboratory situations involving monochromatic waves.

An important aspect of the model development for the

authors, as engineers, was generality or robustness of the computed results. Therefore an effort was made to find forms of empirical coefficients that can be specified with limited information. In most model calibration exercises, the bottom friction coefficient c_f was used as the main fitting parameter. Our examination of three possible forms of the friction coefficient (the commonly used constant, the value of which is somewhat obscure; the *Jonsson* [1966] wave friction coefficient; and the Manning friction coefficient adopted from open-channel flow) showed that the Manning friction coefficient produced agreement as good as or better

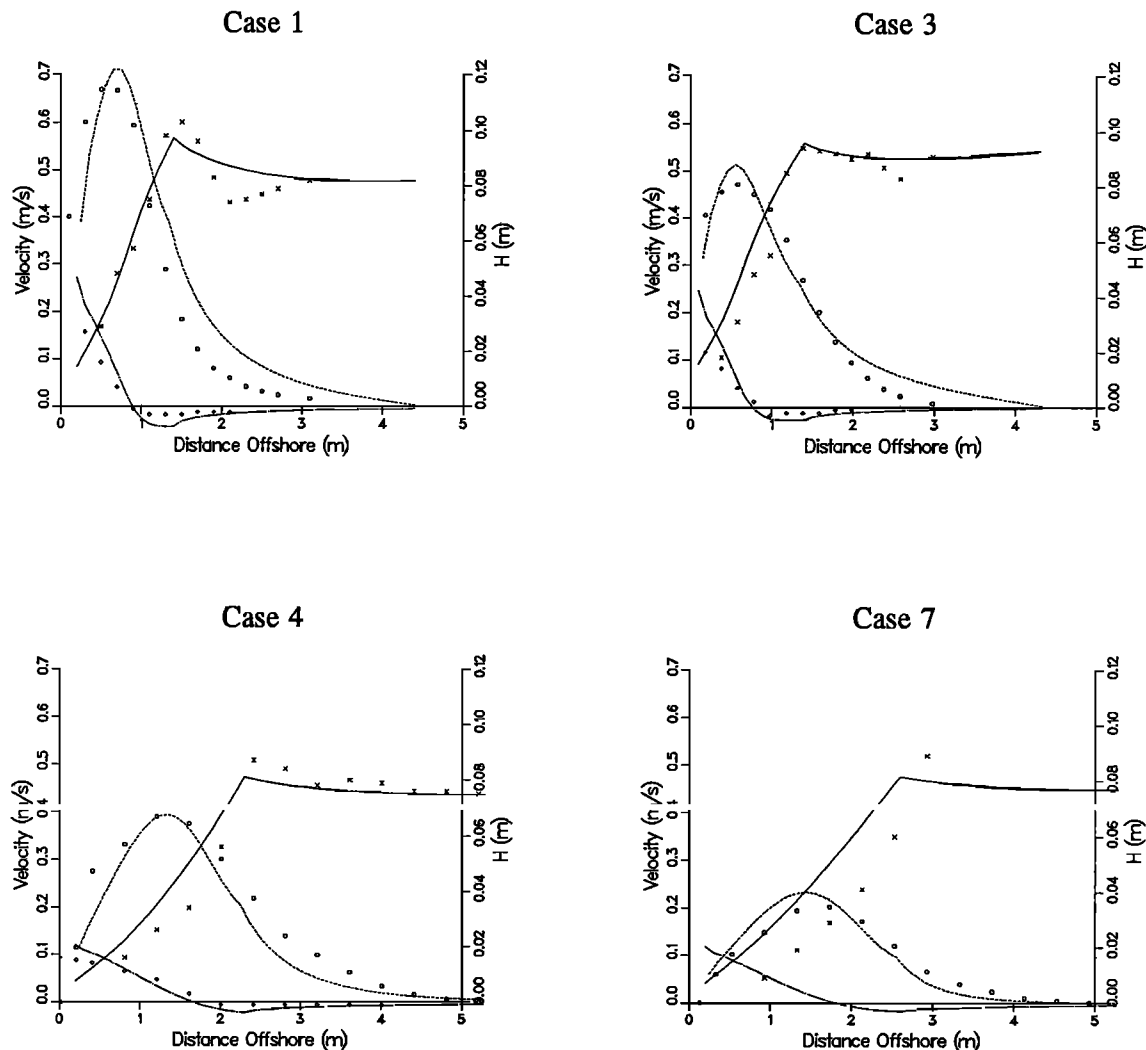


Fig. 11. Comparison of five-equation model wave transformation (solid curves), longshore current (dashed curves), and mean water level (chain-dot curves) calculations to the Visser [1984] laboratory data.

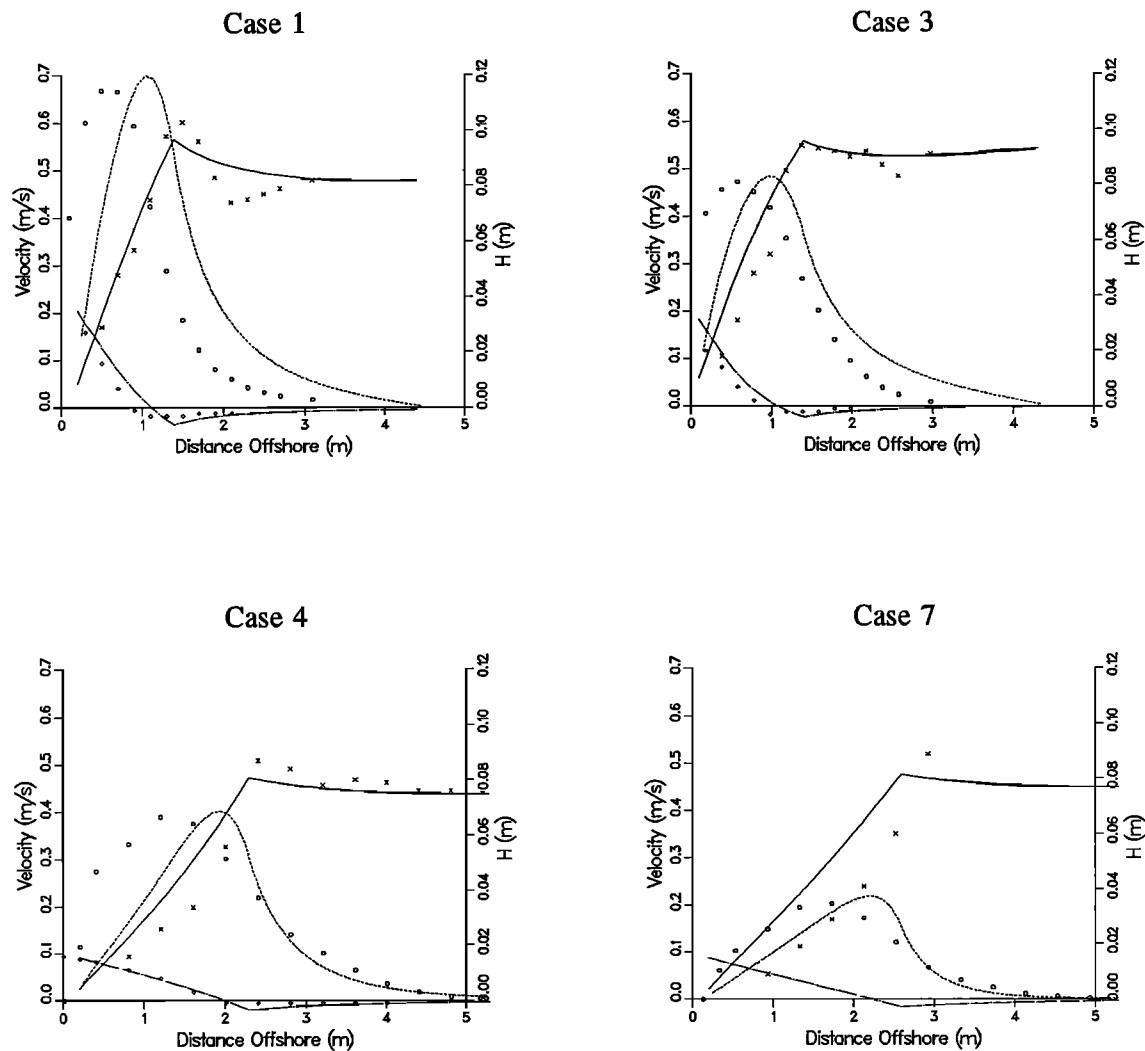


Fig. 12. Comparison of four-equation model wave transformation (solid curves), longshore current (dashed curves), and mean water level (chain-dot curves) calculations to the Visser [1984] laboratory data.

than the other friction coefficients. Values of the empirical Manning resistance coefficient n for three bottom roughnesses (fine sand in the field, smooth and rough concrete in the laboratory) obtained in fitting corresponded well with mean values that are customarily used in open-channel flow. Good correspondence indicates that use of the Manning friction coefficient in longshore current modeling may substantially reduce uncertainty in specification of bottom friction and more objective and reliable prediction if verification data are not available.

Acknowledgments. The DELILAH field data collection project was conducted at the Coastal Engineering Research Center's (CERC's) FRF under the direction of William Birkemeier. The collection of the high-quality data set was accomplished through the expert planning and execution of the multiinstitutional experiment by the FRF staff (Bill Birkemeier, Kent Hathaway, Chuck Long, Gene Bichner, Brian Scarborough, Mike Leffler, Cliff Baron, Carl Miller, Steve Blanchard, and Dawn Miller), Bill Grogg (CERC), Ed Thornton and Rob Wyland (Naval Postgraduate School), Katie Scott (University of California, Santa Cruz), Bob Guza (Scripps Institution of Oceanography), Joan Oltman-Shay (Quest Integrated, Inc.), and Rob Holman, Peter Howd, Todd Holland, and Tom Lippman (Oregon State University). The authors appreciate the

comments of the anonymous reviewers, which stimulated us to revise our original model of the TKE contribution to the momentum equations. The research presented in this paper was conducted under the Nearshore Waves and Currents work unit of Coastal Program and under the Calculation of Boundary Layer Processes work unit of the Dredging Research Program of the Coastal Engineering Research Center, U.S. Army Engineer Waterways Experiment Station. Permission to publish this paper was granted by the Office, Chief of Engineers.

REFERENCES

- Allender, J. H., J. D. Ditmars, W. Harrison, and R. A. Paddock, Comparison of model and observed nearshore circulation, *Proc. Coastal Eng. Conf.*, 16th, 810-827, 1978.
- Battjes, J. A., Modeling of turbulence in the surf zone, *Proc. Symp. Model. Tec.*, 1975, 1050-1061, 1975.
- Baum, S. K., and D. R. Basco, A numerical investigation of the longshore current profile for multiple bar/trough beaches, *Proc. Coastal Eng. Conf.*, 20th, 971-985, 1986.
- Bowen, A. J., The generation of longshore currents on a plane beach, *J. Mar. Res.*, 27(1), 206-215, 1969.
- Bowen, A. J., and R. A. Holman, Shear instability of the mean longshore current, 1, Theory, *J. Geophys. Res.*, 94(C12), 18,023-18,030, 1989.
- Bowen, A. J., D. L. Inman, and V. P. Simmons, Wave "set-down" and set-up, *J. Geophys. Res.*, 73(8), 2569-2577, 1968.

- Chow, V. T., *Open Channel Hydraulics*, 680 pp., McGraw-Hill, New York, 1959.
- Dally, W. R., Random breaking waves: A closed-form solution for planar beaches, *Coastal Eng.*, 14, 233–263, 1990.
- Dally, W. R., R. G. Dean, and R. A. Dalrymple, Wave height variation across beaches of arbitrary profile, *J. Geophys. Res.*, 90(C6), 11,917–11,927, 1985.
- Dalrymple, R. A., Longshore current with wave current interaction, *J. Waterw. Port. Coastal Ocean Div. Am. Soc. Civ. Eng.*, 117(WW4), 414–420, 1980.
- Deigaard, R., P. Justesen, and F. Fredsoe, Modeling of undertow by a one-equation turbulence model, *Coastal Eng.*, 15, 431–458, 1991.
- Ebersole, B. A., and R. A. Dalrymple, Numerical modeling of nearshore circulation, *Proc. Coastal Eng. Conf.*, 17th, 2710–2725, 1980.
- Howd, P. A., and W. A. Birkemeier, Beach and nearshore survey data: 1981–1984 CERC Field Research Facility, *Tech. Rep. CERC-87-9*, 143 pp., U.S. Army Eng. Waterw. Exp. Stn., Vicksburg, Miss., 1987.
- Howd, P., T. Bowen, R. Holman, and J. Oltman-Shay, Infragravity waves, longshore currents, and linear sand bar formation, *Proc. Coastal Sediments*, 1991, 72–84, 1991.
- James, I. D., A non-linear theory of longshore currents, *Estuarine Coastal Mar. Sci.*, 2(3), 235–249, 1974.
- Jonsson, I. G., Wave boundary layers and friction factors, *Proc. Coastal Eng. Conf.*, 10th, 127–148, 1966.
- Komar, P. D., and J. Oltman-Shay, Nearshore currents, in *Handbook of Coastal and Ocean Engineering*, vol. 2, pp. 651–680, edited by J. Herbich, Gulf, Houston, Tex., 1990.
- Kraus, N. C., and M. Larson, NMLONG: Numerical model for simulating the longshore current, *Tech. Rep. DRP-91-1*, 166 pp., U.S. Army Eng. Waterw. Exp. Stn., Vicksburg, Miss., 1991.
- Kraus, N. C., M. Mimura, and K. Horikawa, Investigations of dispersion in and around the surf zone (in Japanese), *Proc. Jpn. Coastal Eng. Conf.*, 27th, 173–177, 1980.
- Larson, M., and N. C. Kraus, Numerical model of longshore current over bar and trough beaches, *J. Waterw. Port Coastal Ocean Eng.*, 117(4), 326–347, 1991.
- Lauder, B. E., and D. B. Spalding, *Mathematical Models of Turbulence*, 169 pp., Academic, San Diego, Calif., 1972.
- Longuet-Higgins, M. S., Longshore currents generated by obliquely incident sea waves, 1, *J. Geophys. Res.*, 75(33), 6778–6789, 1970a.
- Longuet-Higgins, M. S., Longshore currents generated by obliquely incident sea waves, 2, *J. Geophys. Res.*, 75(33), 6790–6801, 1970b.
- Longuet-Higgins, M. S., and R. W. Stewart, Radiation stress in water waves: A physical discussion, with applications, *Deep Sea Res.*, 11, 529–562, 1964.
- McGuirk, J. J., and W. Rodi, A depth-averaged mathematical model for the flow field of side discharges into open-channel flow, *J. Fluid Mech.*, 86, 761–781, 1978.
- Mei, C. C., *The Applied Dynamics of Ocean Surface Waves*, 740 pp., John Wiley, New York, 1983.
- Nadaoka, K., A fundamental study on shoaling and velocity field structure of water waves in the nearshore zone, *Tech. Rep. 36*, Dep. of Civ. Eng., Tokyo Inst. of Technol., Tokyo, Japan, 1986.
- Nairn, R. B., J. A. Roelvink, and H. N. Southgate, Transition zone width and implications for modeling surfzone hydrodynamics, *Proc. Coastal Eng. Conf.*, 22nd, 68–81, 1990.
- Nishimura, H., Numerical simulation of nearshore circulations (in Japanese), *Proc. Jpn. Conf. Coastal Eng.*, 29th, 333–337, 1982.
- Nishimura, H., Computation of nearshore current, in *Nearshore Dynamics and Coastal Processes*, edited by K. Horikawa, pp. 271–291, University of Tokyo Press, Tokyo, Japan, 1988.
- Oltman-Shay, J., P. A. Howd, and W. A. Birkemeier, Shear instabilities of the mean longshore current, 2, Field observations, *J. Geophys. Res.*, 94(C12), 18,031–18,042, 1989.
- Pawka, S. S., Island shadows in wave directional spectra, *J. Geophys. Res.*, 88(C4), 2579–2591, 1983.
- Putrevu, U., and I. A. Svendsen, Wave induced nearshore currents: A study of the forcing, mixing and stability characteristics, *Res. Rep. CACR-91-11*, 242 pp., Cent. for Appl. Res., Univ. of Del., Newark, 1991.
- Rastogi, A. K., and W. Rodi, Predictions of heat and mass transfer in open channels, *J. Hydraul. Div. Am. Soc. Civ. Eng.*, HY3, 397–420, 1978.
- Rodi, W., Turbulence models and their application in hydraulics—A state of the art review, *Sonderforschungsbereich 80*, 140 pp., Inst. für Hydromech., Univ. of Karlsruhe, Karlsruhe, Germany, 1980. (Also printed under the same title by International Association for Hydraulic Research, Delft, Netherlands, 1980.)
- Roelvink, J. A., and M. J. F. Stive, Bar-generating cross-shore flow mechanisms on a beach, *J. Geophys. Res.*, 94(C4), 4785–4800, 1989.
- Sawaragi, T., and K. Iwata, On wave generation after breaking, *Proc. Coastal Eng. Conf.*, 14th, 481–497, 1974.
- Stive, M. J. F., and H. G. Wind, Cross-shore mean flow in the surf zone, *Coastal Eng.*, 10, 325–340, 1986.
- Svendsen, I. A., Wave heights and set-up in the surf zone, *Coastal Eng.*, 8, 303–329, 1984.
- Svendsen, I. A., Analysis of surf zone turbulence, *J. Geophys. Res.*, 92(C5), 5115–5124, 1987.
- Svendsen, I. A., P. A. Madsen, and J. B. Hansen, Wave characteristics in the surf zone, *Proc. Coastal Eng. Conf.*, 16th, 520–539, 1978.
- Symonds, G., and D. A. Huntley, Waves and currents over a nearshore bar system, in *Proceedings Canadian Coastal Conference*, 64–78, National Res. Council Canada, Ottawa, 1980.
- Thieke, R. J., and R. J. Sobey, Cross-shore wave transformation and mean flow circulation, *Coastal Eng.*, 14, 387–415, 1990.
- Thornton, E. B., Variation of longshore current across the surf zone, *Proc. Coastal Eng. Conf.*, 12th, 291–308, 1970.
- Thornton, E. B., and R. T. Guza, Transformation of wave height distribution, *J. Geophys. Res.*, 88(C10), 5925–5938, 1983.
- Thornton, E. B., and R. T. Guza, Surf zone longshore currents and random waves: Field data and models, *J. Phys. Oceanogr.*, 16, 1165–1178, 1986.
- Townsend, A. A., *The Structure of Turbulent Shear Flow*, Cambridge University Press, New York, 1976.
- Van Dorn, W. G., Set-up and run-up in shoaling breakers, *Proc. Coastal Eng. Conf.*, 19th, 738–751, 1976.
- Visser, P. J., The proper longshore current in a wave basin, *Rep. 82-1*, 86 pp., Dept. of Civ. Eng., Delft Univ. of Technol., Delft, Netherlands, 1982.
- Visser, P. J., Uniform longshore current measurements and calculations, *Proc. Coastal Eng. Conf.*, 19th, 2192–2207, 1984.
- Visser, P. J., Laboratory measurements of uniform longshore currents, *Coastal Eng.*, 15, 563–593, 1991.
- WAMDI Group, The WAM model: A third generation ocean wave prediction model, *J. Phys. Oceanogr.*, 18, 1775–1810, 1988.

N. C. Kraus, Conrad Blucher Institute for Surveying and Science, Texas A&M University—Corpus Christi, 6300 Ocean Drive, Corpus Christi, TX 78412.

M. Larson, Department of Water Resources Engineering, University of Lund, Box 118, S-22100, Lund, Sweden.

J. M. Smith, U.S. Army Engineer Waterways Experiment Station, CEWES-CR-P, 3909 Halls Ferry Road, Vicksburg, MS 39180.

(Received February 18, 1992;
revised April 28, 1993;
accepted June 25, 1993.)